Precision Engineering 51 (2018) 499–513

Contents lists available at ScienceDirect

Precision Engineering

journal homepage: www.elsevier.com/locate/precision

Theory and design of spherical oscillator mechanisms☆

I. Vardi[a,*], L. Rubbert[b], R. Bitterli[a], N. Ferrier[a], M. Kahrobaiyan[a], B. Nussbaumer[a], S. Henein[a]

[a] EPFL IMT, Instant-Lab Neuchatel, Switzerland
[b] INSA, Strasbourg, France

ARTICLE INFO

Keywords:
Compliant mechanisms
Conceptual design
Kinematics
Spring designs
Springs
Mechanical oscillators
Analytical dynamics
Euler angles
Listing's law
Eye movements
Constant velocity joint
Chronometry
Isochronism

ABSTRACT

In previous work, we showed that two degree of freedom oscillators can be advantageously applied to horological time bases since they can be used to eliminate the escapement mechanism. We subsequently examined planar two degree of freedom oscillators based on parallel flexure stages. We noted that these oscillators are strongly affected by the orientation of gravity so are not directly suitable for portable timekeepers such as wristwatches. In this paper we examine the design and performance of two degree of freedom spherical oscillators. By spherical oscillator, we mean a spherical mass having purely rotational kinematics and subject to elastic restoring torque. As opposed to our previously examined oscillators, the oscillation period of spherical oscillators is relatively insensitive to the effect of tilting the mechanism in the presence of gravity. In order to restrict spherical rotation to two degrees of freedom, we restrict the kinematics to obey Listing's law, a well-known constraint occurring in human eye movement. We show that a particular central restoring force we call the scissors law is best suited for chronometric performance and propose a number of theoretical mechanisms producing it. We then design an actual spherical oscillator based on our theoretical results. The design uses flexure springs to restrict kinematics to Listing's law, produce the scissors law and provide the necessary suspension. Finally, we present experimental data based on a physical realization indicating promising chronometric performance.

1. Introduction

1.1. Oscillator time-bases without escapement

The biggest improvement in timekeeper accuracy was due to the introduction of the oscillator as a time base, first the pendulum by Christiaan Huygens in 1656 [18], then the balance wheel-spiral spring by Huygens and Hooke in about 1675, and the tuning fork by N. Niaudet and L.C. Breguet in 1866 [26]. Since that time, these have been the only mechanical oscillators used in mechanical clocks and in all watches, see the survey [27].

In [14], we presented new time bases for mechanical timekeepers which, in their simplest form, were based on a harmonic oscillator first described in 1687 by Isaac Newton in *Principia Mathematica* [25,Book I,Proposition X]. This oscillator is the isotropic harmonic oscillator, where a mass m at position $\mathbf{r}$ is subject to a central linear restoring force (Hooke's law), and as Newton showed, the resulting trajectories are elliptical (Fig. 2). More significantly for our purposes, Newton showed that trajectories are isochronous, that is, the frequency of rotation is the same for all orbits. Since isochronism is the basis of precision timekeeping, such oscillators are ideal candidates for mechanical timekeepers, however, it appears that this has not been previously constructed or even proposed [15].

Since trajectories have unidirectional rotation, these oscillators have the advantage of solving the problem of inefficiency of the escapement by eliminating it completely [14]. Unidirectional rotational motion is the key to eliminating the escapement, and this desirable property is achieved by passing from the one degree of freedom oscillators found in classical time keepers: pendulum, balance wheel, tuning fork, to two degree of freedom mechanical oscillators having a *central force,* that is, a restoring force towards a unique stable position. In practice, the escapement mechanism is replaced by a crank which is driven by the energy storage mechanism such as a watch mainspring and which then maintains and counts time base oscillations by a pin attached to the oscillator, see [14,15].

☆ Second revision submitted to Precision Engineering, September 20, 2017.

* Corresponding author.
E-mail addresses: ilan.vardi@epfl.ch (I. Vardi), lennart.rubbert@insa-strasbourg.fr (L. Rubbert), roland.bitterli@epfl.ch (R. Bitterli), nicolas.ferrier@epfl.ch (N. Ferrier), mohammad.kahrobaiyan@eplf.ch (M. Kahrobaiyan), billy.nussbaumer@epfl.ch (B. Nussbaumer), simon.henein@epfl.ch (S. Henein).

http://dx.doi.org/10.1016/j.precisioneng.2017.10.005
Received 2 March 2017; Received in revised form 20 September 2017; Accepted 9 October 2017
Available online 18 October 2017

Fig. 1. Clock with time base our spherical oscillator.

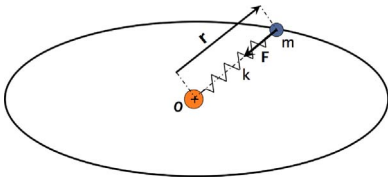

Fig. 2. Elliptical orbit under central Hooke law.

1.2. Specifications for an oscillator for time-base without escapement

The ultimate goal is to have a time base for a mechanical wristwatch which requires excellent isochronism which means following Newton's model as closely as possible. The model assumes a point mass and, as described in [14], a positive angular momentum yields an isochronism defect, so any mass rotational inertia should be eliminated.

Wristwatches are portable timekeepers so the oscillator should be insensitive to gravity and to shocks.

These considerations lead to the following specifications for an oscillator time-base for a mechanical watch without escapement

1. A two degree of freedom oscillator.
2. A linear restoring force, i.e., which obeys Hooke's law.
3. A central restoring force, i.e., the spring potential has a unique minimum.
4. The central restoring force is *isotropic,* i.e., it is the same in all radial directions.
5. The mobile mass behaves as a particle, i.e., as a point mass.
6. Motion is restricted to a plane.
7. Mass is independent of position.
8. Chronometric accuracy is insensitive to oscillator energy (isochronism).
9. Chronometric accuracy is insensitive to gravity and shocks.

1.3. Spherical oscillators

In a previous article [30], we focused our attention to planar two degree of freedom oscillators based on configurations of X–Y stages, which were designed to very closely satisfy the first eight conditions but which does not at all satisfy condition 9. This makes it very suitable as a clock time-base and the authors built a prototype clock which has been on exhibit at the Neuchatel, Switzerland, city hall since December 2016 [9]. However, failure to satisfy condition 9 makes this oscillator design unsuitable for portable timekeepers.

We therefore turned our attention to spherical oscillators which do satisfy condition 9. By *spherical oscillator,* we mean a spherical mass having purely rotational kinematics and subject to elastic restoring torque. Since the center of gravity of the mass is immobile during oscillation, the oscillator period is relatively insensitive to the effect of tilting the mechanism in the presence of gravity.

Not all specifications of Section 1.2 can be respected, since for spherical oscillators motion is no longer planar (condition 6). Since Newton's model does not hold, it follows that our oscillator is no longer isochronous (condition 8). We do manage to retain a weaker form of isochronism by considering what happens at stable circular orbits. Such orbits always occur for central forces and we show that replacing Hooke's law (condition 1) by what we have called the scissors law produces isochronism of stable circular orbits.

The isotropy defect of our constructed oscillator was not optimized and this is the subject of our ongoing research. Our constructed oscillator thus satisfies conditions 3, 5, 7 and potentially 9.

We therefore note that the above specifications were used as a guideline for constructing an oscillator and the object of our study is to design an oscillator with sufficient chronometric performance to be used as a time-base for a wristwatch. Experimental tests of our design indicates that this is indeed the case.

We constructed a clock with the spherical oscillator described in this paper and shown in Fig. 1. This fully functional clock will be exhibited at the International Museum of Horology, La Chaux-de-Fonds, Switzerland, in September 2017 [22].

Remark. Spherical oscillator time bases were previously considered in the early 1960s by the CEH, the Swiss research group which invented the quartz watch, but they were unable to find acceptable methods of suspending the sphere and maintaining oscillations . This paper effectively solves this problem.

1.4. Outline of the paper

We first examine the theoretical aspects of spherical oscillators. Due to the remarkable similarity with eye movements, which are spherical rotations, we will adopt much of the notation of eye movements. In fact, our results here have led to applications to eye movements [16].

Since the sphere with fixed center has three degrees of freedom, condition 1 requires a restriction to two degrees of freedom. This is accomplished by specifying that the kinematics of our spherical oscillator respect *Listing's law,* which is well-known to apply to human eye movement.

We analyze the kinematics and dynamics of spherical rotation under Listing's law. We will show that the dynamics are essentially that of a point mass, i.e., condition 5 above.

We then examine potentials corresponding to central restoring forces and we show that there is a unique potential producing isochronism for stable circular orbits. Due to its physical realization, we call this the *scissors law.*

We then describe theoretical mechanisms realizing the kinematics. We show that Listing's law can be realized by a constant velocity joint and our restoring force by a scissors mechanism. We then show that the scissors restoring force can also be realized by a constant velocity joint and $N \geq 3$ evenly distributed equatorial linear springs, and this has the advantage of eliminating spring circular motion present in our initial scissors mechanism.

We then proceed to the design of an actual spherical oscillator. A physical design requires limiting kinematics to Listing's law, springs producing the scissors law as well as suspension to hold the sphere. We based our design on the equatorial realization by having three equally

distributed equatorial beams. The first point is that this beam placement almost eliminates torsion, so the kinematics closely follow Listing's law and constructing a complicated CV joint is avoided. Secondly, the beams approximate linear springs, so the restoring force approximates the scissors law without any spurious spring motion. Finally, the polar beam provides the required suspension.

Our design is not quite faithful to the theoretical mechanism so we model the behavior of our equatorial beams to estimate the isotropy defect of our restoring force as well as its discrepancy from the ideal scissors law. In fact, the numerical data of Section 3.2.5 indicates that our mechanism does not approximate the scissors law, due to the effect of the polar beam suspension.

Finally, we describe our actual construction of the three equatorial beam spherical oscillator and present experimental data indicating that our demonstrator has an acceptable isochronism defect.

The structure of the paper is summarized by

- Study the analytic theory of spherical 2-DOF oscillators and theoretical mechanisms realizing their kinematics.
- Use the ideal theoretical mechanisms as an inspiration for a simple mechanical design.
- Provide an analytical model of the design.
- Derive numerical data from the analytical model of the design.
- Construct a physical realization of the design.
- Evaluate the chronometric performance of the physical realization.

2. Theory

2.1. Kinematics

2.1.1. Listing's law

The first specification we address is condition 1 which requires restricting motion to two degrees of freedom. We do this by having our spherical mechanisms obey *Listing's law,* which is a restriction on spherical positions reducing the degree of freedom of rotation to two. Since this concept first appeared in relation to eye movement, we present a brief description of its history.

Three dimensional rotations have three degrees of freedom and do not commute, so total freedom of eye position could conceivably cause problems, since eye orientation for a given line of sight could depend on the path chosen to reach it, causing different retinal images (this can indeed occur [34]). It was first suggested by Donders [8] that in some situations, each given line of sight corresponds to a unique eye orientation and eliminating path dependence. This was subsequently named *Donders' Law* by Helmholtz in Volume III of his treatise of physiological optics [12]. Donders' Law is the exact statement that spherical rotations are limited to two degrees of freedom.

A more explicit description of possible eye positions was given by Johannes Benedict Listing (1808–1882),[1] apparently without any physical evidence nor subsequent publication, the statement is given below. This constraint was subsequently named *Listing's Law* by Helmholtz [12], see [29] for surveys of the subject, [36] for experimental confirmation, it is known in robotics as a zero torsion mechanism for spherical rotation [4]. Though Listing's Law is generally thought to be a method of restricting the degree of freedom of the eye from three to two in order to avoid orientational confusion, this is not entirely obvious, as explained by Tweed [33]. Listing's Law restricts the possible orientations as follows.

Listing's law. There is a direction called the *primary position* so that any *admissible* position is obtained from this position by a rotation whose axis is perpendicular to the direction of the primary position.

It follows that all axes of rotation lie on a single plane which we call the *Listing plane.* In Section 2.2, we will consider dynamics of the sphere under the Listing constraint and we will call *admissible motion* one passing only through admissible Listing positions.

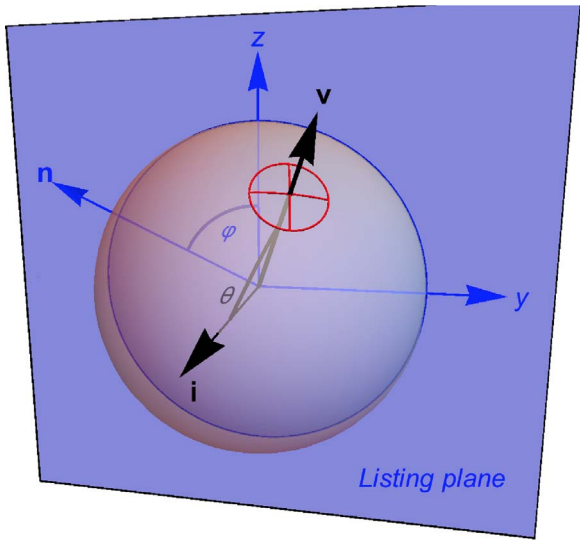

Fig. 3. Eye looking in **v** direction: vector **n** in the Listing plane is axis of rotation of eye by angle θ.

2.1.2. Notational conventions

Since our models follow Listing's law and this restriction has been the subject of active research in the field of eye movement, we have decided to follow the notational convention of the eye in which the primary position is pointing in the x direction and the z direction is pointing vertically up, that is, opposite to the gravitational force (Fig. 3).

We will also freely use reference to eye movement, in particular, we use the term *line of sight* to mean the modified position of the point (1, 0, 0) under rotation. We use the term *torsion* to mean a rotation around the line of sight.

Unless otherwise indicated, we will assume that the sphere radius equals 1. We let the primary position be such that the line of sight points to the positive x axis. We will denote the point $\mathbf{i} = (1, 0, 0)$ as the primary position since there is only one admissible rotation with that line of sight. With these coordinates, the y–z plane becomes the *Listing plane* containing all admissible rotational axes. Any such rotational axis can be taken to be the z-axis rotated around the x-axis by an angle φ, so represented by the unit vector $\mathbf{n} = (0, -\sin\varphi, \cos\varphi)$. One then rotates around $\mathbf{n}$ by an angle θ taking the front pole $\mathbf{i}$ to the point $\mathbf{v} = (\cos\theta, \sin\theta\cos\varphi, \sin\theta\sin\varphi)$, the $\mathbf{v}$ direction thus becomes the current line of sight. This expresses the fact that any admissible Listing position is described by the spherical coordinates (θ, φ) corresponding to the Euclidean coordinates $(\cos\theta, \sin\theta\cos\varphi, \sin\theta\sin\varphi)$ of the resulting line of sight $\mathbf{v}$, as calculated above. It is important to note that θ is *colatitude,* so our coordinate system may differ from other definitions of spherical coordinates.

As will be seen in Section 2.2.1, it is natural to decompose rotations into *radial motion* in θ and *circular motion* in φ, see Fig. 4. Admissible motion in θ with φ fixed moves either directly towards or directly away from the primary position, so is radial motion. We will also call θ the *tilt angle,* a notation consistent with the term "tip-tilt mechanism" well-known in the literature.

Motion in φ with θ fixed keeps a constant distance from the primary position, so is circular motion. The decomposition is analogous to polar coordinates in the plane. This interpretation is physically consistent with θ and φ as *generalized coordinates* and will be the basis for our dynamical analysis of Section 2.2.

Finally, we use the notation $\mathbf{R}(\alpha, \mathbf{a})$ to denote a rotation by angle α around the axis $\mathbf{a}$. The rotation $\mathbf{R}(\alpha, \mathbf{a})$ is applied to vectors on the right,

[1] Listing's most famous discovery, the Möbius strip, is better known by the name of its co-discoverer.

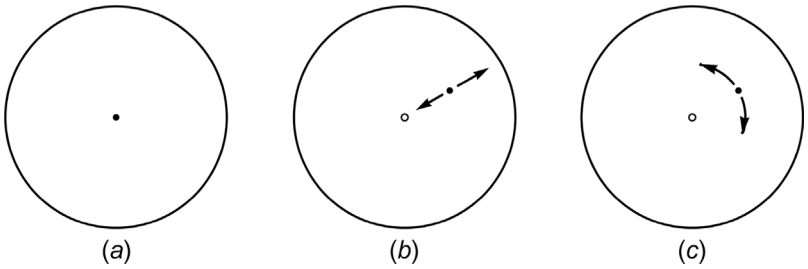

Fig. 4. Motion viewed from **i** direction: (a) primary position, (b) radial motion (tilt), (c) circular motion.

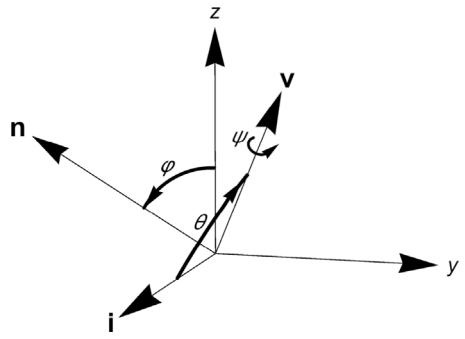

Fig. 5. Euler angles sequence of rotations φ, θ, ψ.

so vector **u** is rotated by $\mathbf{R}(\alpha, \mathbf{a})$ to obtain vector **v** according to $\mathbf{v} = \mathbf{u}\,\mathbf{R}(\alpha, \mathbf{a})$. This is consistent with using row vectors and the 3×3 matrix representation for rotations, with rotation of vectors by matrix multiplication.

2.2. Dynamics

Listing's Law gives a set of constraints on possible sphere rotations. The standard method of analyzing the dynamics of mechanical systems under a set of constraints is to appeal to *analytical dynamics,* that is using φ, θ as generalized coordinates and replacing Newton's Laws and vectors in favor of energy considerations, see [10,32,38] for a description. This will require a computation of the kinetic energy and therefore of the angular velocity vector, and the most direct approach appears to be Euler angles.

2.2.1. Euler angles

To analyze Listing's Law, we appeal to the well-known Euler angle formulation of rigid body rotation, see . Using the notation of the previous section, any rotation of a rigid body is expressed by three angles φ, θ, ψ (Fig. 5): a rotation of angle φ around **i** taking the z-axis vector **k** to **n**, followed by a rotation of angle θ around **n** taking **i** to **v**, followed by a rotation of angle ψ around **v**.[2] In terms of the notation defined in Section 2.1.2, this is the product $\mathbf{R}(\varphi, \mathbf{i})\,\mathbf{R}(\theta, \mathbf{n})\,\mathbf{R}(\psi, \mathbf{v})$.

In our case, it is easily seen that a Listing position (θ, φ) is obtained by the Euler angles φ, θ, $-\varphi$, that is, $\psi = -\varphi$. In terms of Section 2.1.2, this says that an admissible Listing rotation is the composition of rotations

$$\mathbf{R}(\varphi, \mathbf{i})\,\mathbf{R}(\theta, \mathbf{n})\,\mathbf{R}(-\varphi, \mathbf{v}). \tag{2.2.1.1}$$

This relation among the Euler angles of Listing positions is not usually presented in the literature, though it is stated by Helmholtz without any emphasis or accompanying figures. Moreover, the Euler angle formulation is essentially: "torsion, rotation without torsion, undo torsion," so spurious torsion is introduced by Euler angles. It follows Euler angles are counter-intuitive and are probably not a faithful model of the physiological mechanism. However, they are used here because they radically simplify the formulation of the eye's angular velocity by reducing it to a single line.

One of the main applications of Euler angles is to provide an explicit formula for the angular velocity $\boldsymbol{\omega}$ of a rotating body and it is well-known that, due to additivity of infinitesimal rotations,[3] that the composition of rotations given by $\mathbf{R}(\varphi, \mathbf{i})$, $\mathbf{R}(\theta, \mathbf{n})\,\mathbf{R}(\psi, \mathbf{v})$ can be quite simply derived term by term to give

$$\boldsymbol{\omega} = \dot{\varphi}\mathbf{i} + \dot{\theta}\mathbf{n} + \dot{\psi}\mathbf{v}.$$

Our case is $\psi = -\varphi$, so the angular velocity of admissible Listing rotations is given by

$$\boldsymbol{\omega} = \dot{\varphi}(\mathbf{i} - \mathbf{v}) + \dot{\theta}\mathbf{n}. \tag{2.2.1.2}$$

Remark. The Euler angle convention is to call φ, θ, ψ *precession*, *nutation*, and *spin*. Listing circular motion therefore corresponds exactly to "precession exactly opposite spin." In the case of the Earth, this would mean that the 26,000 year precession cycle would speed up to a 23 h 56 min sidereal day.

2.2.2. Energy considerations

In order to set up the Lagrangian formulation of the dynamics, one begins by computing the kinetic energy of the system. Assume that the mass density is spherically symmetric so the moment of inertia of the mass is given by the single scalar I, then the kinetic energy is $K = I \parallel \boldsymbol{\omega} \parallel^2/2$. Formula (2.2.1.2) gives

$$\|\boldsymbol{\omega}\|^2 = \dot{\varphi}^2\|\mathbf{i} - \mathbf{v}\|^2 + \dot{\theta}^2,$$

since **n** is a unit vector orthogonal to $\mathbf{i} - \mathbf{v}$, so that

$$K = \frac{I}{2}(\dot{\theta}^2 + 4\sin^2(\theta/2)\dot{\varphi}^2).$$

Given a potential $V(\theta, \varphi)$, the Lagrangian is

$$\mathscr{L} = K - V = \frac{I}{2}(\dot{\theta}^2 + 4\sin^2(\theta/2)\dot{\varphi}^2) - V(\theta, \varphi). \tag{2.2.2.1}$$

The generalized momentums are

$$p_\theta = \frac{\partial \mathscr{L}}{\partial \dot{\theta}} = I\dot{\theta}, \quad p_\varphi = \frac{\partial \mathscr{L}}{\partial \dot{\varphi}} = 4I\sin^2(\theta/2)\dot{\varphi},$$

confirming that θ resembles radial motion, since p_θ is analogous to standard linear momentum of a particle moving in Euclidean space, while p_φ is analogous to angular momentum of such a particle (though both p_θ and p_φ are actually angular momentum).

In analogy with the central forces examined by Newton, we restrict ourselves to *central potentials,* by which we mean potentials which do not depend on φ and $\dot{\varphi}$. In this case, p_φ is a constant, usually written L in this context, and this generalized angular momentum L is preserved. In particular, this implies that for sufficiently small θ, if motion is not

[2] The standard sequence is to rotate with respect to **k**, **j**, **v**, but this has been modified here since the primary position point in direction **i** instead of **k**.

[3] It appears that the derivation of the angular velocity given in [35,equations (19)–(24)] is essentially the proof of additivity of angular velocity, compare with [23,Proof of Theorem 9.3,p. 374]. Additivity also implies that infinitesimal rotations commute, compare with [21,28]. See [2,p. 42–44] for a geometric proof of the additivity of infinitesimal rotations.

perfectly radial, $\dot{\varphi}(t) \neq 0$ for some t, then trajectories orbit around the primary position without ever attaining it. This is the unidirectional motion required for our time bases without escapement.

Given a central potential $V(\theta)$, one expresses $\dot{\varphi}$ in terms of $L = p_\varphi$ to derive an expression for the total energy

$$E = K + V = \frac{I}{2}\left(\dot{\theta}^2 + \frac{L^2}{4I^2\sin^2(\theta/2)}\right) + V(\theta). \tag{2.2.2.2}$$

This energy formula is similar to the spherical pendulum, in which case V is the gravitational potential, see [20,38] for a complete explicit solution to the dynamics of the spherical pendulum in terms of elliptic functions. Using similar methods, we were able to compute explicit solutions in terms of elliptic functions to our problem in the special case of the scissors potential of Section 2.3.4.

In further announced work [16], we have shown that the dynamics are equivalent to the dynamics of a point mass on an associated two dimensional sphere of unit quaternions. This goes to show that our model satisfies condition 5 of the specifications of Section 1.2.

2.3. Circular isochronism

Since our spherical oscillators do not follow Newton's model, isochronism of arbitrary orbits is no longer possible so we consider a restricted form.

Definition. We define *circular isochronism* to mean that circular steady state orbits all have the same period.

Note that there are steady-state circular orbits since we only consider central potentials. We will consider possible central potentials V and examine the behavior of circular steady state orbits, in other words, orbits with constant θ and constant $\dot{\varphi}$. For every angle θ, there exists a circular constant angular speed $\dot{\varphi}$ satisfying the equations of motion, the corresponding period is $T(\theta) = 2\pi/\dot{\varphi}$.

Definition. By *circular isochronism defect* we mean the relative discrepancy $T(\theta)/T_0 - 1$ of circular steady state orbits at angle θ, where T_0 is a nominal period.

2.3.1. General circular orbits

Consider a general central potential V and the corresponding Lagrangian of Eq. (2.2.2.1). The Euler–Lagrange equation in θ is

$$\frac{d}{dt}\left(\frac{\partial \mathscr{L}}{\partial \dot{\theta}}\right) = \frac{\partial \mathscr{L}}{\partial \theta}$$

which gives the equation of motion

$$I\ddot{\theta} - I\dot{\varphi}^2\sin\theta + \frac{\partial V}{\partial \theta} = 0.$$

For steady state circular orbits $\ddot{\theta} = 0$ and $\dot{\varphi}$ is a constant. This gives the following equation for steady state circular motion

$$\dot{\varphi} = \sqrt{\frac{1}{I\sin\theta}\frac{\partial V}{\partial \theta}},$$

confirming that $\dot{\varphi}$ is constant for any fixed value of θ. The corresponding steady-state period is

$$T(\theta) = 2\pi\sqrt{I\sin\theta \Big/ \frac{\partial V}{\partial \theta}}. \tag{2.3.1}$$

2.3.2. Linear restoring force

The simplest analogy with the planar case examined by Newton is a linear central restoring force with potential $V_\ell = \kappa\theta^2/2$, so that

$$\frac{\partial V_\ell}{\partial \theta} = \kappa\theta$$

and formula (2.3.1) says that the period of constant rotational motion is

$$T(\theta) = 2\pi\sqrt{\frac{I\sin\theta}{\kappa\theta}}. \tag{2.3.1.1}$$

Note that $T_0 = 2\pi\sqrt{I/\kappa}$ is the period of the classical one dimensional rotational harmonic oscillator with stiffness κ and restoring torque I. Taking as nominal period the value of T_0 in Eq. (2.3.1.1) gives

$$\frac{T(\theta)}{T_0} = \sqrt{\frac{\sin\theta}{\theta}}.$$

The right hand side of the previous equation has the series expansion

$$\sqrt{\frac{\sin\theta}{\theta}} = 1 - \frac{1}{12}\theta^2 + \mathscr{O}(\theta^4),$$

so the circular isochronism defect is

$$\frac{T}{T_0} - 1 = -\frac{1}{12}\theta^2 + \mathscr{O}(\theta^4).$$

2.3.3. Comparison with pendulums

It is interesting to compare the circular isochronism defect of the linear restoring force to the well-known classical isochronism defect for the simple pendulum

$$\frac{T(\theta)}{T_0} - 1 = \frac{1}{16}\theta^2 + \mathscr{O}(\theta^3),$$

and the circular isochronism defect of the conical pendulum

$$\frac{T(\theta)}{T_0} - 1 = -\frac{1}{4}\theta^2 + \mathscr{O}(\theta^3).$$

The performance of the linear restoring force is therefore inferior to the classical pendulum, though superior to the conical pendulum. We conclude that linear restoring force is not a promising candidate for a time base.

2.3.4. Scissors law restoring force

It turns out that there is a particular central potential which eliminates the isochronism defect of steady-state circular orbits for our model, the *scissors potential* $V_s = \kappa\sin^2(\theta/2)$, with constant κ. The name "scissors potential" comes from the spring mechanism described in Section 2.4.3 which generates this potential. Since

$$\frac{\partial V_s}{\partial \theta} = \frac{1}{2}\kappa\sin\theta$$

Formula (2.3.1) for steady state orbits yields

$$T(\theta) = 2\pi\sqrt{\frac{2I}{\kappa}},$$

which is a constant so circular isochronism holds. This justifies the statement that this potential is the correct choice for our model.

Remark. The total energy formula (2.2.2.2) for the scissors potential is

$$E = \frac{I}{2}\left(\dot{\theta}^2 + \frac{L^2}{4I^2\sin^2(\theta/2)}\right) + \kappa\sin^2(\theta/2). \tag{2.3.3.1}$$

2.4. Theoretical mechanisms

2.4.1. State of the art

The description of Listing positions given by Euler angles in Section 2.2.1, i.e., that spin is exactly opposite precession, suggested to us a new model and a new mechanism for Listing's law, described Section 2.4.2 below. We begin by reviewing previous mechanizations.

Simple mechanisms modeling eye rotation were proposed by Fick and Helmholtz using gimbals, but these do not respect Listing's Law, see [5,p. 150] [11].

A physical realization was first observed by Nakayama [24] who noted that Listing rotations could be induced via the bending of an

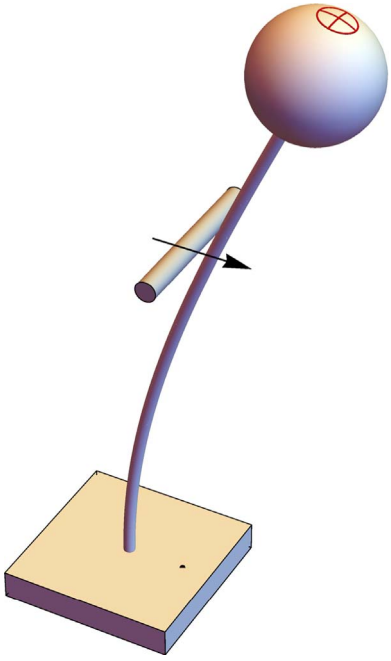

Fig. 6. An isotropic beam producing Listing rotations of the sphere around its center.

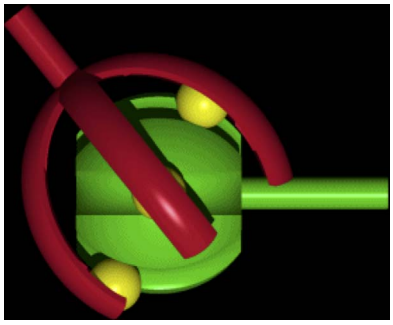

Fig. 7. An Rzeppa constant velocity joint [6].

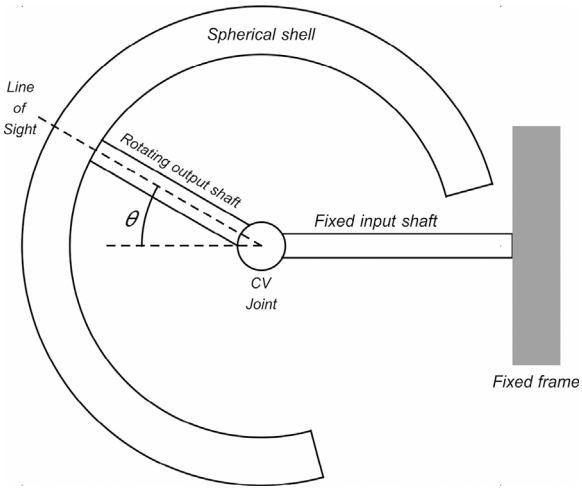

Fig. 8. CV joint realization of Listing's law.

isotropic object, i.e., whose elastic restoring force is the same in all directions. His example consisted of an isotropic membrane holding a rigid beam. We have modified this mechanism slightly by using an isotropic beam, see Fig. 6. Applying a force causes it to bend with the sphere at its extremity rotating around its center according to Listing's

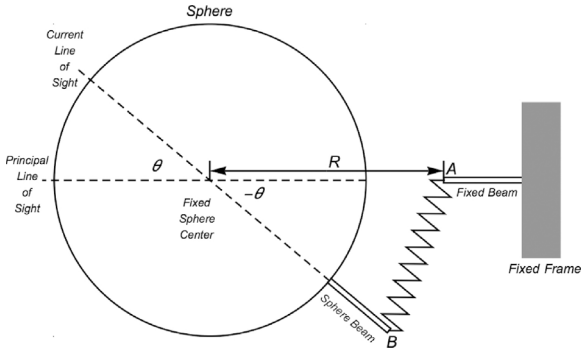

Fig. 9. Spring applies a force of magnitude $2k\,R\sin(\theta/2)$ on B towards A.

Law. This realization is not pursued here since it has the defect of translating the sphere.

2.4.2. Constant velocity joint realization of Listing's law

A mechanical realization of Listing's Law is possible using *constant velocity joint,* usually abbreviated *CV joint.* These are variants of the universal joint, in which a cylindrical rod enters the joint at a given axial rotation speed, and a cylindrical rod exiting the joint at an arbitrary angle has the same axial rotation speed. An example of a constant velocity joint is given in Fig. 7, see the patent for details [31]. Constant velocity joints have numerous automotive applications, but it does not appear that this mechanism has been proposed as a physical implementation of Listing's Law.

To see how this implements Listing's Law, a spherical shell representing the eye is rigidly attached to the output shaft, where the output shaft axis corresponds to the line of sight. The constant velocity joint is situated at the center of the spherical shell, with the output shaft able to rotate freely in radial motion as in the convention of Fig. 4, for angles $0 \le \theta < \theta_{\max}$, e.g., $\theta_{\max} = 45^\circ$. The output shaft can also rotate freely about its axis. Fig. 8 gives a cross-sectional view of this mechanism, where spin occurs around the input shaft axis and precession around the output shaft, so both of these are rotations out of the page.

The construction is such that the input shaft is attached to a fixed frame and does not rotate. We then consider a rotation of the sphere around this fixed input shaft, where the angle of the output shaft θ is constant. Note that this corresponds to precession. Since the input shaft is fixed, the CV joint causes an opposite and equal rotation of the sphere around the output shaft, corresponding to spin. Therefore, precession and spin are exactly opposite which is the exact condition for circular admissible motion and Listing circular motion is achieved. Since Listing radial motion is free, this mechanism realizes Listing's Law.

2.4.3. A mechanical realization of the scissors law

The central potential of Section 2.3.4 can be physically realized by the mechanism shown in Fig. 9. The mechanism provides a restoring force to bring the eye back towards the principal position. It is situated behind the eye so as not to interfere with vision but an equivalent construction consists of transposing the mechanism to the front of the eye. Despite any similarity to the construction of Fig. 8, the mechanism is independent of the constant velocity joint realization of Listing's law of that figure, and the mechanism described here applies to a general physical realization of sphere rotation.

The basic mechanism illustrated in Fig. 9 is a linear spring joining A and B, where A is a fixed position in the negative direction of the principal position, so behind the occipital point, and B in the negative direction of the current line of sight so rotating with the radial angle $-\theta$. Both A and B are placed at the same distance R from the center of the sphere. The construction is such that the attachments are unaffected by sphere rotation, i.e., the spring rotates around A with sphere precession and is not affected by sphere spin at B. It is also assumed that the spring is in its neutral position when the sphere is in the principal

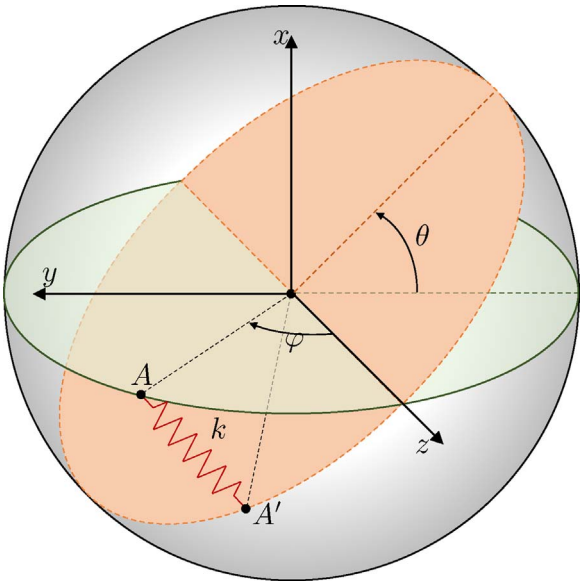

Fig. 10. Linear spring attached to the equatorial plane of the sphere.

at distance R from the sphere center, this gives a torque, or generalized force, $-kR^2 \sin\theta$. Using the fact that a potential V generates the generalized force $-\partial V/\partial\theta$, this gives $V = 2kR^2 \sin^2(\theta/2)$, yielding the potential V_s defined in Section 2.3.4, with $\kappa = 2kR^2$.

2.4.4. Equatorial springs realization of the scissors law

The realization of the scissors law of the previous section has the defect that the spring mechanism is on the polar axis so the spring mechanism itself rotates under circular motion. We address this issue by showing that for a sphere with rotations restricted to Listing Law, $N \geq 3$ identical equally distributed equatorial linear springs produce a scissors law restoring torque acting towards the principal position. Here we assume that the springs have zero free length when the sphere is in its primary (neutral) position.

We begin by considering a single spring. Without loss of generality, we assume that the sphere has radius 1 and that the spring is placed at the point **A** on the equator at an angle φ measured clockwise from the z axis in the y–z plane, see Fig. 10. Since the spring is assumed to be linear with zero free length, a displacement $\mathbf{A} \mapsto \mathbf{A'}$ produces a restoring force $k(\mathbf{A} - \mathbf{A'})$, where k is the spring stiffness.

We now consider what happens when the sphere is tilted by an angle θ, where, without loss of generality, this rotation can be assume

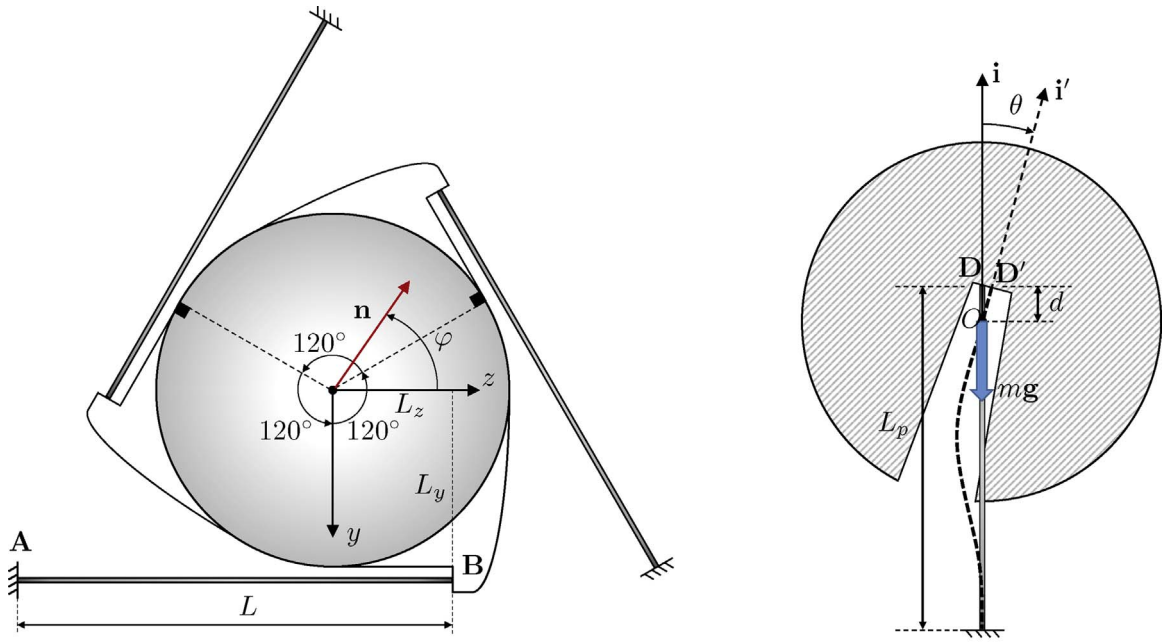

(a) Top view. (b) Side view.

Fig. 11. Schematic design depicting the three equatorial beams (a) and the polar beam (b).

position, i.e., when A coincides with B.[4]

At radial angle θ, elementary trigonometry shows that the spring length is $2R\sin(\theta/2)$, see Fig. 9, so extended by this amount from its neutral position at $A = B$. The spring then exerts a force $-2k\,R\sin(\theta/2)$ at B and towards A, where k is the spring constant. Neglecting axial compression force on the sphere beam, the resulting force at B is the projection of the spring force in the direction orthogonal to the sphere beam, and this equals $-2k\,R\sin(\theta/2)\cos(\theta/2) = -\,k\,R\sin\theta$. Since B is to be around the z axis. Explicitly, the attached point goes from $\mathbf{A} = (0, \sin\varphi, \cos\varphi)$ to $\mathbf{A'} = (-\sin\theta\sin\varphi, \cos\theta\sin\varphi, \cos\varphi)$.

The lever arm at $\mathbf{A'}$ is the projection $\mathbf{L} = (-\sin\theta\sin\varphi, \cos\theta\sin\varphi, 0)$ of $\mathbf{A'}$ onto the x–y plane so the restoring torque is the cross product $\mathbf{L} \times k(\mathbf{A} - \mathbf{A'})$. A direct computation shows that

$$\mathbf{L} \times k(\mathbf{A} - \mathbf{A'}) = (0,\, 0,\, -k\sin^2\varphi\sin\theta),$$

so the torque resulting from a single spring at angle φ to the z-axis results in a restoring torque $-k\sin^2\varphi\sin\theta$ about the z-axis.

In the case of N evenly distributed equatorial springs, the previous result shows that the total torque is given by

$$-k\sin\theta\sum_{m=0}^{N-1}\sin^2\left(\varphi + \frac{2\pi m}{N}\right).$$

[4] This is a conceptual construction which is not physically correct since the spring is not physically supported and the neutral position indicated requires that the spring be attached at a fixed position distinct from A, in the direction opposite B. However, an actual physical realization having the exact properties is easily obtained. Note that a physical realization requires that spring and sphere do not intersect, so $R\cos(\theta/2) \geq 1$ which shows that his mechanism only works for a radial angle bounded away from π.

Table 1
Parameter values.

I	L	L_p	r	L_y	L_z	E	ν
1.23×10^{-3} kgm^2	112 mm	70 mm	0.5 mm	45 mm	41 mm	210 GPa	0.3

The sum on the right is easily shown to equal $N/2$ when $N \geq 3$, for example, as proved using the identities $\sin^2 t = (1 - \cos 2t)/2$ and $e^{it} = \cos t + i \sin t$, and expressing the sum in terms of the real part of a geometric series [19]. It follows that the total restoring torque due to the $N \geq 3$ springs is

$$-\frac{kN}{2}\sin\theta,$$

which is a scissors law, since k and N are constants.

3. Design

3.1. Description of the design

A physical realization of a theoretical mechanism must approximate the theoretical kinematics, Listing's Law, and also approximate a scissors restoring torque. Moreover, the mechanism must also have a suspension, as it operates under a gravitational field and this is achieved using flexures (compliant mechanisms) [13,17].

Our design has three equatorial beams, which restrict the kinematics and produce a restoring torque. In addition, a single polar beam is added to provide an adequate suspension for the mechanism. All the beams have uniform circular cross sections of radius r. Following a well-known result of Wittrick [39], we suspend the sphere on the polar beam above the center of the sphere at a ratio of 1/8 above center and 7/8 below center in order to minimize the parasitic shift of the center in the x direction, so $d = L_p/8$ in Fig. 11(b). The three equatorial beams are arranged by a 120° consecutive rotation about the center O in the equatorial plane (y, z plane, see Fig. 11). This arrangement is inspired by the equatorial spring mechanism of Section 2.4.4 which indicates that this setup has a good chance of approximating the scissors law.

Since our model only uses three equatorial springs and one spring as a suspension, it appears to be the simplest possible realization of a spherical oscillator obeying Listing's Law and approximating a scissors law.

3.1.1. Design parameter values

The following Table 1 gives the values used for our design and the construction described in Section 4.1.

3.1.2. Assumptions

We make two assumptions which imply that our mechanism restricts rotations to a good approximation to Listing's Law. The first assumption is that our four beams have infinite axial stiffness. In the principal position, the three co-planar equatorial beams suppress all in plane motion including torsion (rotation around the polar axis), while the polar beam suppresses the out-of-plane translation. The second assumption is that the tilt angle is small so that the previous argument remains valid up to first order and sphere translation and torsion around the tilted polar axis are negligible. Since torsion is suppressed for these small angles, Listing's Law holds in this range.

3.1.3. Outline of results and computations

We construct an analytical model based on Euler–Bernoulli theory, as described in Section 3.3, which provides a theoretical estimate for the restoring torque of each beam under a Listing rotation. Adding these torques gives an estimate of the restoring torque for three equatorial beams and the polar beam.

This allowed us to estimate the isotropy defect of our model. Note that the polar beam is inherently isotropic since it is axial in the principal position **i** and has circular cross-section, so the isotropy defect depends only on the three equatorial beams.

We also made a finite element simulation using COMSOL of the

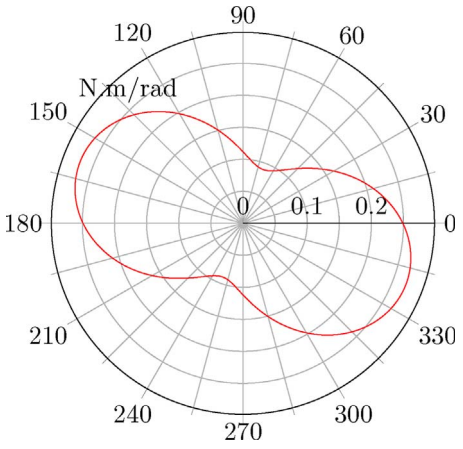

Fig. 12. Single equatorial beam normalized restoring torque around **n** as function of φ and $\theta = 1°$.

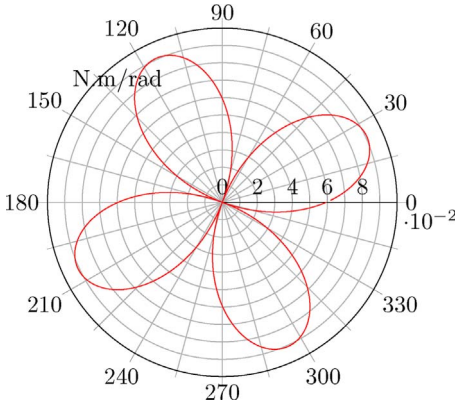

Fig. 13. Single equatorial beam normalized restoring torque around **m** as function of φ and $\theta = 1°$.

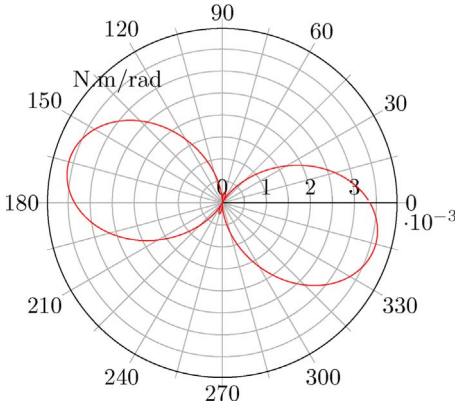

Fig. 14. Single equatorial beam normalized restoring torque around **i** as function of φ and $\theta = 1°$.

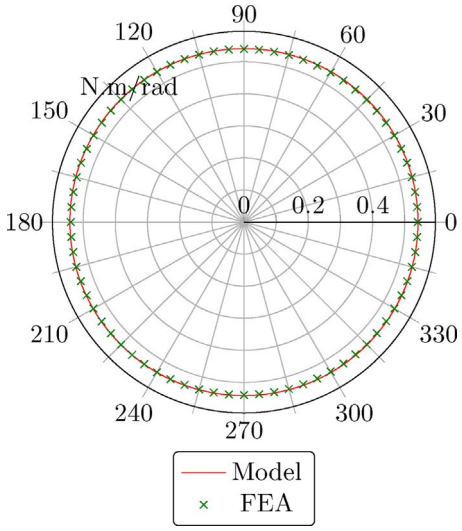

Fig. 15. Normalized restoring torque of three equatorial beams around **n** as a function of φ for $\theta = 1^\circ$.

three beam model and the four beam model under standard gravity and compared the isotropy defect.

Finally, we compared the stiffness of our model with scissors law stiffness. Note that we have used the term *normalized restoring torque* instead of stiffness, as this is a more precise description, see Section 3.2.1 below.

3.2. Numerical results

In order to get directly to our results, we first present our numerical results based on the computations of Section 3.3. We start with data computed for a single equatorial beam, then proceed to the case of three equatorial beams and finally three equatorial beams and the polar beam.

3.2.1. Single equatorial beam

Applying a tilt angle θ around **n**, we define the *normalized restoring torque* of a single equatorial beam around **n**, **m** and **i** as the restoring torque of that beam around **n**, **m** and **i** divided by θ. Figs. 12–14 represent these for φ ranging from 1° to 360° in 1° increments and tilt angle $\theta = 1^\circ$. Here $\mathbf{m} = \mathbf{i} \times \mathbf{n}$, see Section 3.3.2. The exact values are not important, since we expect significant cancellation when considering three evenly spaced equatorial beams. However, we still

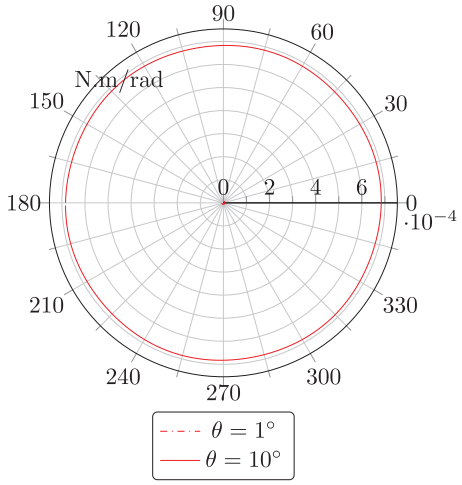

Fig. 16. Normalized restoring torque of three equatorial beams around **m** as a function of φ for $\theta = 1^\circ$ and $\theta = 10^\circ$.

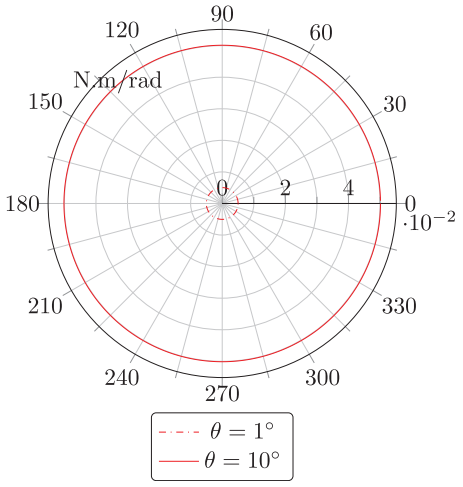

Fig. 17. Normalized restoring torque of three equatorial beams around **i** as a function of φ for $\theta = 1^\circ$ and $\theta = 10^\circ$.

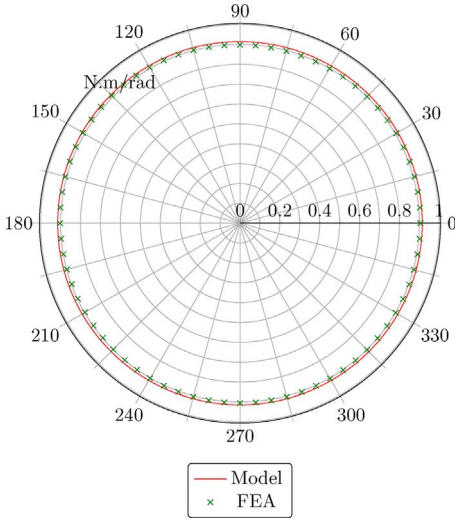

Fig. 18. Normalized restoring torque of three equatorial beams and polar beam around **n** as a function of φ, under gravity and for $\theta = 1^\circ$.

provide this data in order to present our approach.

3.2.2. Three equatorial beams

We took the data given in Section 3.2.1 and added it for three equatorial beams shifted by 120°. Figs. 15–17 give the total normalized restoring torque, respectively, around the **n**, **m** and **i** axes for angle φ from 1° to 360° in 1° increments.

We note that Fig. 15 only shows the result for $\theta = 1^\circ$, the data for $\theta = 10^\circ$ was virtually identical. Figs. 16 and 17 show that normalized restoring torque for $\theta = 1^\circ$ is much smaller than for $\theta = 10^\circ$.

The theory outlined in Section 2 requires that normalized restoring torque only depends on the tilt angle θ, that is, on rotations around **n**. It is therefore desirable for the contributions of the **m** and **i** normalized restoring torques to be small compared to the **n** normalized restoring torque.

Figs. 15–17 show that for $\theta = 1^\circ$, the **m** and **i** normalized restoring torques are 0.0013% and 0.9292%, respectively, of the **n** normalized restoring torque.

For $\theta = 10^\circ$, **m** and **i** normalized restoring torques are 0.1296% and 9.2824%, respectively, of the **n** normalized restoring torque.

3.2.3. Three equatorial beams and polar beam

We now add to the data of Section 3.2.2 the normalized restoring

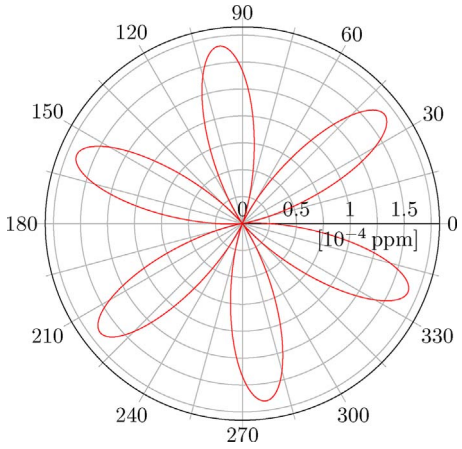

Fig. 19. Isotropy defect ε_φ of four beams around **n**, $\theta = 1^\circ$.

torque due to the polar beam, as computed in Section 3.3.3. We note that the polar beam has zero torsion, so it only contributes restoring torque to tilt around **n**. It follows that the graphs shown in Figs. 16 and 17 remain the same, so we only present Fig. 18, the modified version of Fig. 15.

Once again, we wish to compare the **n** normalized restoring torque to the **m** and **i** normalized restoring torques. Fig. 18 with Figs. 16 and 17 show that for $\theta = 1^\circ$, the **m** and **i** normalized restoring torques are 7.42×10^{-4}% and 0.5501%, respectively, of the **n** normalized restoring torque.

For $\theta = 10^\circ$, the **m** and **i** normalized restoring torques are 0.0750% and 5.4832%, respectively, of the **n** normalized restoring torques.

These numerical values characterize the defect from our ideal theoretical design. This defect seems negligible.

3.2.4. Comparison with scissors law: isotropy

The scissors law requires an isotropic restoring torque, since it does not depend on the circular angle φ.

We evaluate isotropy by taking the stiffness values k_φ around **n**, i.e., the normalized restoring torques as defined in Section 3.2.1, which are shown in Fig. 18 and looking at the relative error $\varepsilon_\varphi = (k_\varphi - k_{\min})/k_{\min}$, for $\varphi = 1^\circ, 2^\circ, \ldots, 360^\circ$, where $k_{\min}$ is the minimal value of k_φ.

Fig. 19 shows that for tilt angle $\theta = 1^\circ$, the relative isotropy defect ε_φ is less than 1.68×10^{-4} ppm. A similar computation $\theta = 10^\circ$ shows that the relative isotropy defect is less than 1.68 ppm.

We conclude that isotropy holds up to a very small error.

3.2.5. Comparison with scissors law: stiffness

The scissors law requires the restoring force to be proportional to $\sin\theta$, so that stiffness with respect to rotation around an axis **n** in the y–z plane is proportional to $\sin\theta/\theta$. Recall that this stiffness is actually the normalized restoring torque as defined in Section 3.2.1 and, by abuse of notation, we use to the word "stiffness" in this section, since it is the usual term, and no confusion should result.

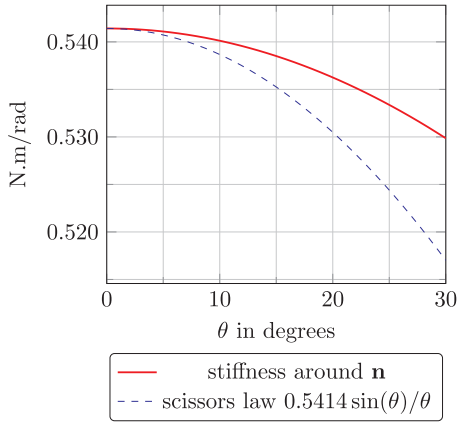

Fig. 20. Three equatorial beam stiffness around **n**.

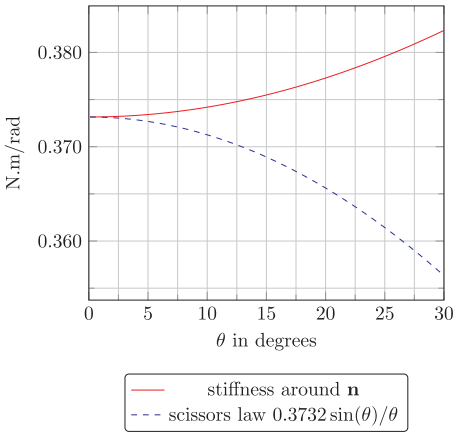

Fig. 21. Polar beam stiffness behavior around **n**.

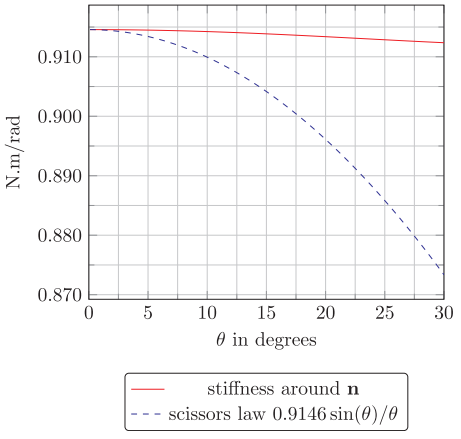

Fig. 22. Four beam stiffness around **n**.

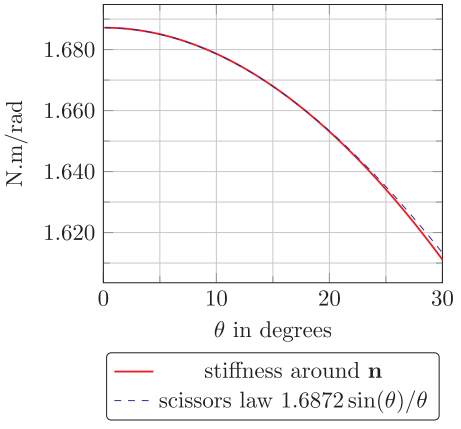

Fig. 23. Four beam stiffness around **n** for $L_y = 90$ mm and $L_z = 56$ mm.

The fact that isotropy holds up to small error, as shown in Section 3.2.4, means that we can study the stiffness for an arbitrary angle φ and the results will hold in general.

The actual stiffness should be computed by the sum of stiffnesses around **n**, **m** and **i**. For the purposes of this paper, we only consider stiffness around **n** and make the assumption that the induced error is negligible.

Fig. 20 compares the 3-beam stiffness around **n** with a best fit

scissors law. The numerical data seems to indicate that our three beam model is a fair approximation to the scissors law.

The stiffness numerical data of the polar beam is shown in Fig. 21 indicating that it does not at all respect a scissors law.

Finally, the stiffness data of all four beams is shown in Fig. 22 indicating that the overall restoring torque is more close to the linear restoring torque than the scissors law restoring torque.

Our numerical simulation indicates that, in term of stiffness, our design does not respect a scissors law. Hence, we expect circular isochronism defect for our design which will be less than the isochronism defect of a design with linear restoring torque discussed in Section 2.3.2.

Remark. It appears that our design can be further improved to closely follow the scissors law. In particular, setting $L_y = 90$ mm and $L_z = L/2 = 56$ mm results in a very good approximation of scissors law as illustrated in Fig. 23.

3.3. Analytical model

Having assumed Listing's Law and Euler–Bernoulli beam theory, we derive analytical formulas to compute the restoring torque of the equatorial and polar beams.

The physical situation is inherently nonlinear and we note that our model only takes some nonlinearity into account:

- At the tip of a beam, the restoring moment and shear force are nonlinear functions of the bending angle and deflection which leads to nonlinearity of the beam stiffness. Our analytical model, does not take this nonlinearity into account, i.e., we assume that the bending moment and shear force are linear functions of the bending angle and deflection.
- At the tip of the beams attached to the sphere, the bending angle, torsion angle and deflection are nonlinear functions of the sphere tilt angle θ, which leads to nonlinearity of the stiffness of our mechanism. Our analytical model taken this nonlinearity into account.
- The center of rotation **O** undergoes a parasitic shift during oscillation which affects the stiffness of our mechanism. Our model neglects the effect of parasitic shift in the equatorial plane. However, the parasitic shift along the polar axis is taken into account since effect of gravity along this parasitic shift affects the stiffness of the polar beam.

3.3.1. Restoring torque

We use an explicit vectorial approach to derive expression for restoring torque under a spherical tilt. We take a unit sphere with center at the origin $\mathbf{O} = (0, 0, 0)$ rigidly attached to an arm lying on the equatorial plane with end tip at point $\mathbf{B} = (0, L_y, L_z)$. As in Section 2.1.1, we assume Listing's Law holds with the respect to the principal position $\mathbf{i} = (1, 0, 0)$ with all admissible positions corresponding to rotations with axis on the y–z plane. Any admissible rotational axis can be taken to be the z-axis rotated around the x-axis by an angle φ represented by the vector $\mathbf{n} = (0, -\sin\varphi, \cos\varphi)$. One then rotates around $\mathbf{n}$ by an angle θ taking vector $\mathbf{i}$ to the vector $\mathbf{i}'$.

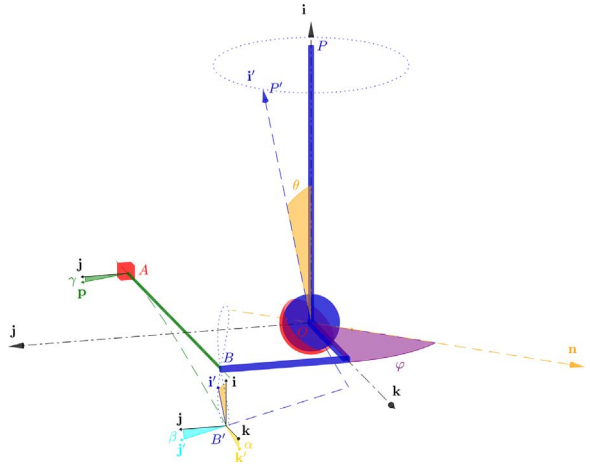

Fig. 24. Notations. View 1.

As in Section 2.1.2, we call rotation in θ radial motion and in φ circular motion. Under pure circular motion, $\mathbf{i}'$ describes a circle of radius $\sin\theta$ while the point $\mathbf{B}'$ describes a Fig. 8-shaped curve on a sphere of radius $\|\mathbf{OB}\|$.

Recall the notation of Section 2.1.2 expressing a rotation of angle α around axis $\mathbf{a}$ as $\mathbf{R}(\alpha, \mathbf{a})$ and acting on the right on row vectors. We also use formula (2.2.1.1) stating that the Listing rotation with tilt θ and rotation φ around $\mathbf{n}$ can be expressed as right action by

$$\mathbf{R}(\varphi, \mathbf{i})\,\mathbf{R}(\theta, \mathbf{n})\,\mathbf{R}(-\varphi, \mathbf{i}'), \quad \text{where } \mathbf{i}' = \mathbf{i}\,\mathbf{R}(\theta, \mathbf{n}).$$

3.3.2. Single equatorial beam

Our equatorial beam is taken to be a cantilever Euler–Bernoulli beam of length L with uniform circular cross-section of radius r (Fig. 24). Without loss of generality, we assume that the beam at its resting position is parallel to the z axis, rigidly fixed at $\mathbf{A} = (0, L_y, L_z - L)$ and attached to the sphere at $\mathbf{B} = (0, L_y, L_z)$. It is assumed that the beam undergoes no tension or compression.

The tilt θ in the φ direction imposes a change in position and orientation of the beam tip **B**. The new position is given by $\mathbf{B} \mapsto \mathbf{B}'$ and the new orientation is described by the local frame $\mathbf{i}'$, $\mathbf{j}'$, $\mathbf{k}'$ at the beam tip, where $\mathbf{i} \mapsto \mathbf{i}'$, $\mathbf{j} \mapsto \mathbf{j}'$, $\mathbf{k} \mapsto \mathbf{k}'$.

The *tip bending angle* α is the angle between $\mathbf{k}$ and $\mathbf{k}'$ and the *torsion angle* β is the angle between $\mathbf{j}$ and $\mathbf{j}'$.

Euler–Bernoulli theory says that the displacement and new orientation give rise to a restoring shear force $\mathbf{F}$ and a restoring moment $\mathbf{M}$ due to bending as well as a restoring torque T due to torsion.

The total restoring torque $\boldsymbol{\tau}$ applied to the sphere by the beam is therefore

$$\boldsymbol{\tau} = -\mathbf{B}' \times \mathbf{F} - \mathbf{M} - T\mathbf{k}', \tag{3.3.2.1}$$

where $\mathbf{B}'$ is given by Listing's Law

$$\mathbf{B}' = \mathbf{B}\,\mathbf{R}(\varphi, \mathbf{i})\,\mathbf{R}(\theta, \mathbf{n})\,\mathbf{R}(-\varphi, \mathbf{i}').$$

We now proceed to the computation each of the quantities in formula (3.3.2.1). Due to three dimensional deflection, bending of the beam consists of two bendings which are projections of the deflected beam on the x, z plane, and y, z plane. For the x, z plane bending, we denote the tip deflection and bending angle by f_x and α_y, respectively; and for the y, z plane bending, we denote them by f_y and α_x, respectively, where

$$f_x = \mathbf{BB}'\cdot\mathbf{i}, \quad f_y = \mathbf{BB}'\cdot\mathbf{j}, \quad \alpha_x = \arctan(\mathbf{k}'\cdot\mathbf{j}/\mathbf{k}'\cdot\mathbf{k}), \quad \alpha_y = \arctan(\mathbf{k}'\cdot\mathbf{i}/\mathbf{k}'\cdot\mathbf{k}).$$

One obtains $\mathbf{F}$ and $\mathbf{M}$ by solving the Euler–Bernoulli problem with boundary conditions deflections f_x, f_y and bending angles α_y and α_x at the tip of the beam, yielding

$$\mathbf{F} = \frac{12\mathrm{EI}}{L^3}(f_x, f_y, 0) - \frac{6\mathrm{EI}}{L^2}(\alpha_y, \alpha_x, 0), \quad \mathbf{M} = -\frac{6\mathrm{EI}}{L^2}(-f_y, f_x, 0) + \frac{4\mathrm{EI}}{L}(-\alpha_x, \alpha_y, 0),$$

where $I = \pi r^4/4$ is the area moment of inertia of the beam cross-section and E is the Young modulus.

Saint Venant torsion theory holds, so the torsional torque is well-known to be

$$T = \frac{\mathrm{GJ}}{L}\beta'$$

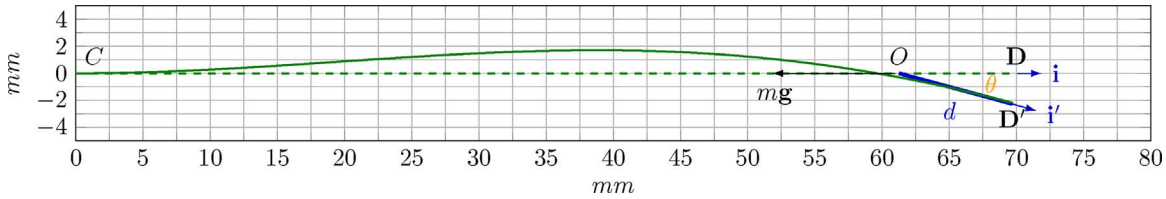

Fig. 25. Detail of polar beam deflection.

where $G = E/(2(1+\nu))$ is the shear modulus with ν the Poisson ratio, $J = \pi r^4/2$ is the polar area moment of inertia of the beam cross-section, and angle $\beta' = \arcsin\{[(0, \cos\alpha_x, -\sin\alpha_x) \times \mathbf{j'}]\cdot\mathbf{k'}\}$.

3.3.3. Polar beam

We now consider the polar beam which lies in the principal direction **i** and which in its nominal position passes through the sphere center **O**. Since the beam acts as the sphere suspension, we assume it is subjected to the force of gravity. Moreover, under a Listing rotation with tilt θ, the tip of the beam **D** is constrained to move in a circle of radius d with center at **O**.

We want to compute the restoring torque around **O** under a Listing rotation with tilt θ. Note that the beam is isotropic, since it has cylindrical cross-section, so we do not have to take the direction φ of the rotational axis into account.

We do this by considering an Euler–Bernoulli beam under compression with boundary conditions given by the above constraints. Hence, the force–displacement relation of the polar beam is [3]

$$\begin{pmatrix} F_p L_p^2/\mathrm{EI} \\ M_p L_p/\mathrm{EI} \end{pmatrix} = \frac{\delta}{2(1-\cos\delta)-\delta\sin\delta} \begin{pmatrix} \delta^2\sin\delta & \delta(\cos\delta-1) \\ \delta(\cos\delta-1) & \sin\delta-\delta\cos\delta \end{pmatrix} \begin{pmatrix} d\sin\theta/L_p \\ \theta \end{pmatrix},$$

where F_p and M_p denote the shear force and the bending moment of the polar beam at the mobile end, respectively. In addition, $\delta = \sqrt{\mathrm{mgL}_p^2/\mathrm{EI}}$ where m is the sphere mass and g is standard gravity (Fig. 25).

Given the shear force and the bending moment of the polar beam, we obtain the restoring torque τ_p (torque around point O) applied by the polar beam to the sphere as follows

$$\tau_p = M_p + F_P d\cos\theta + \mathrm{mgd}\sin\theta.$$

4. Construction and experimental data

4.1. Construction

The oscillator design described in Section 3 was constructed according to the parameter values given in Section 3.1.1 and built on a wooden frame, as shown in Fig. 26.

The sphere was constructed of stainless steel and has radius 40.5 mm. The actual oscillating body consists of the sphere, its impulse pin, pieces to attach the equatorial and polar beams and six assembly screws, yielding total mass 1.79 kg and moment of inertia $I = 1.23 \times 10^{-3}\,\mathrm{kgm}^2$. The extra pieces are why the moment of inertia I is greater than the theoretical moment of inertia $1.17 \times 10^{-3}\,\mathrm{kgm}^2$ given by the sphere formula $2mr^2/5$ with radius 40.5 mm and mass 1.79 kg.

A vertical pin was attached to the top of the sphere, see Fig. 26(a), and, as described in Section 1.1, the oscillator was then maintained by a crank producing torque via an external energy source, as shown in Fig. 27(a). In our case, the energy source was an electric motor Maxon DCX10S EB KL 1.5V, as shown in Fig. 27(b), with angle encoder ENX10 EASY 1024IMP. The electrical current was provided by a Keithley 2460 SourceMeter.

4.2. Chronometry

4.2.1. Chronometry definition

We consider our oscillator and we record times of passage $t_0, t_1, \ldots, t_n$, in seconds, to a specified reference angle as described in Section 4.2.2. This is done over the given time interval t_0 to t_n. One then defines the period $T_i = t_i - t_{i-1}$, for $i = 1, \ldots, n$.

A linear regression is then performed on $t_0, \ldots, t_n$ to get a best linear fit $t_i = T^*i + C$. It follows that T^* is the best linear fit period approximating the T_i, $i = 1, \ldots, n$. Finally, we consider the error with respect to the best fit by considering the values

$$e_i = \frac{86400}{t_n - t_0}(t_i - T^*i - C)$$

which quantify, in seconds per day, the discrepancy from a perfectly regular oscillator with constant period.

4.2.2. Chronometry data

The time values $t_0, \ldots, t_n$ were measured by recording the time of passage of the motor at a specified reference angle. This was done as follows: when the motor is at the specified angle, its encoder sends a signal to an Arduino Uno R2 micro-controller board which records the value c_i of a counter incremented at 32768 Hz by a ChronoDot V2.1 High Precision RTC (Real Time Clock). Thus, the time value t_i is taken to be $c_i/32768$. This introduces a measurement error due to the resolution of the time base. However, it is well-known that such measurements errors do not affect the qualitative data in the long run [1].

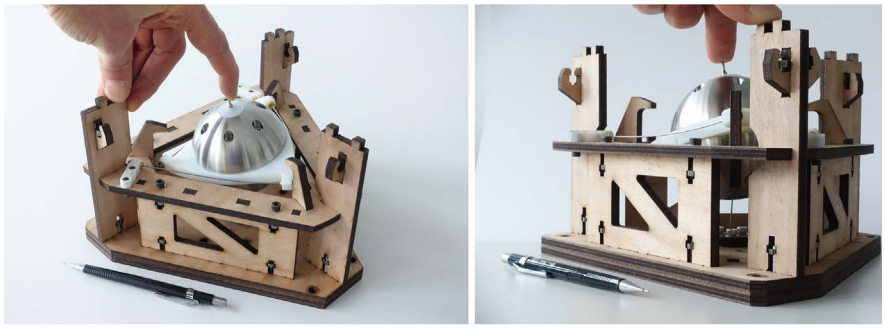

(a) View showing 3 equatorial beams and impulse pin.

(b) Side view showing polar beam.

Fig. 26. Constructed oscillator prototype.

(a) Crank. (b) Electric motor.

Fig. 27. Maintaining mechanism.

A 24 h test was performed which found the best fit period $T^* = 237.76$ ms corresponding to frequency 4.20592 Hz, see Fig. 28. With this best fit estimate, the errors e_i were found to lie between 3s/d and −1.5s/d, as shown in Fig. 29. Note that the model stiffness $k = 0.9146$ N m/rad gives model frequency $1/(2\pi)\sqrt{k/I} = 4.3399$ Hz, which is slightly higher than the experimentally observed frequency.

4.3. Isochronism

4.3.1. Isochronism definition

Isochronism is the basis of timekeeper chronometric performance since it frees the time base from variations of maintaining energy. Maintaining energy is directly proportional to total oscillator energy, the proportionality is essentially the *quality factor Q*, see [37]. It follows that isochronism can be evaluated by seeing how oscillator rate varies as oscillator energy varies.

Remark. The classical definition of isochronism considers oscillator rate with respect to oscillator amplitude [7]. This approach is not suitable here as it is unclear how to define the amplitude. However, our energy definition is equivalent to the classical amplitude approach since in that case energy is proportional to the square of the amplitude, see [37]. In the classical case, the correspondence between energy and amplitude is evident for small amplitude variation by noting that energy variation is double amplitude variation.

Given an oscillator with nominal energy E_0, we compute a nominal best fit period T_0^* by recording periods over a given time interval t and doing a linear fit, as described in Section 4.2.1. We now consider the same oscillator with energy E and record its periods over the same time interval t and obtain a best fit period T^* and define the *daily rate* to be

$$\rho = 86400\frac{T^* - T_0^*}{T^*},$$

expressed in seconds per day. We are interested in how this rate varies as the oscillator energy E varies, so we let $\Delta E = E - E_0$ represent the energy variation and $\Delta E/E$ the relative energy variation. We finally evaluate isochronism by comparing the rate ρ with $E_{\%} = 100\Delta E/E$, the relative energy variation expressed in percentage.

4.3.2. Indirect energy measure

For harmonic oscillators obeying Newton's model described in Section 1, this method is possible since total oscillator energy is proportional to $A^2 + B^2$, where A and B are the major and minor axes of the mass' elliptical trajectory, so relatively easy to measure experimentally.

For our spherical oscillators, however, experimental measurement of total oscillator energy does not appear to be simple since the total energy

$$E = \frac{I}{2}\left(\dot{\theta}^2 + \frac{L^2}{4I^2\sin^2(\theta/2)}\right) + \kappa\sin^2(\theta/2)$$

of the scissors potential, formula (2.3.3.1) derived in Section 2.3.4 is not proportional to any easily measurable quantity. We therefore turn to measurement of maintaining torque which is proportional to total oscillator energy. This can be seen using well-known formulation of energy loss E_r per oscillator period given a quality factor Q, see [37],

$$E_r = \frac{2\pi E}{Q}.$$

We assume a maintaining torque τ allowing the oscillator to keep total energy E, so the work done by the maintaining torque in one oscillator

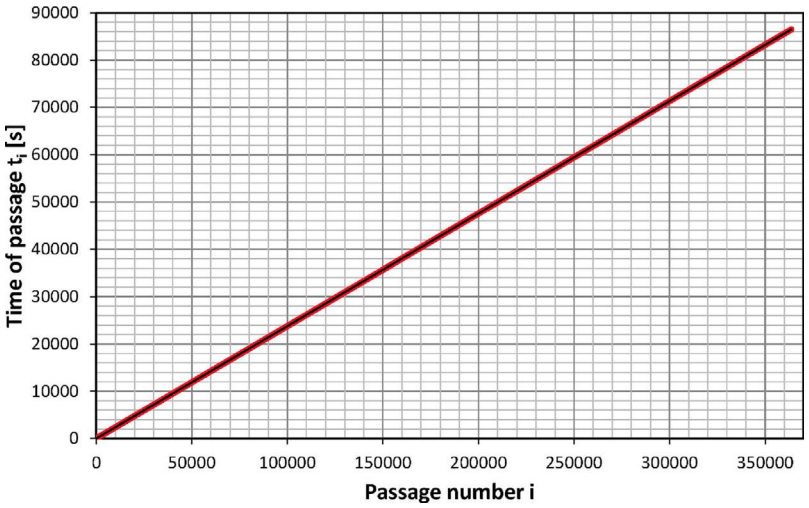

Fig. 28. 24 h chronometry test with linear regression.

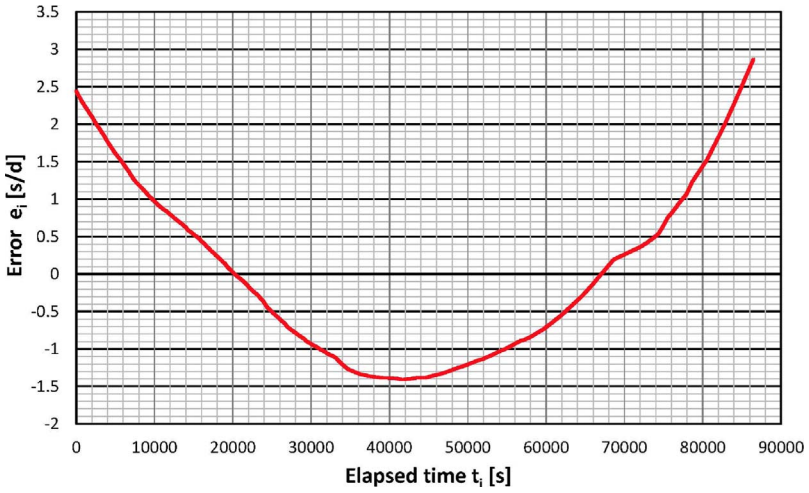

Fig. 29. Time error with respect to best fit period.

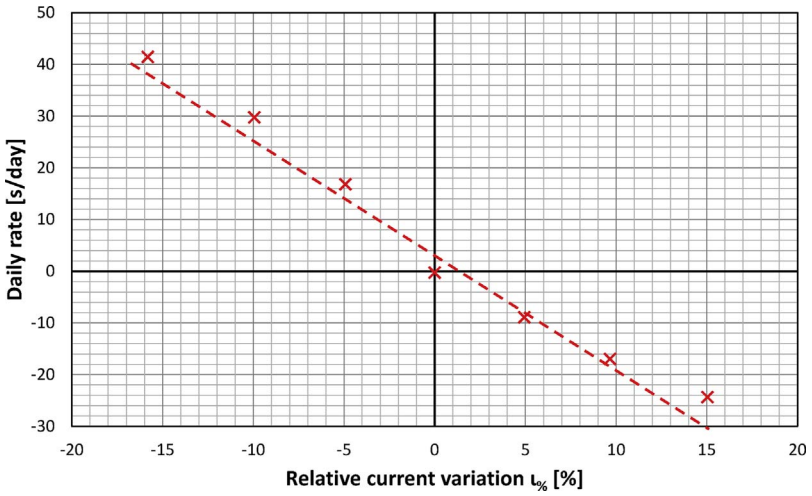

Fig. 30. Daily rate versus estimated relative energy variation.

period is $2\pi\tau$. It follows that

$$E = \tau Q,$$

so total energy is proportional to maintaining torque. Finally, we estimate maintaining torque by assuming it to be proportional to motor current as indicated by the motor controller.

In Section 4.3.1, we defined isochronism as the relation between the rate ρ and the relative energy variation $E_{\%}$ in percent. Based on the above argument, we replace $E_{\%}$ with the relative current variation $\iota_{\%} = 100(\iota - \iota_0)/\iota$, where ι is the current and ι_0 the nominal current.

4.3.3. Isochronism data

The nominal current was taken to be $\iota_0 = 40$ mA and a range of ± 15% of the nominal current was chosen in 5% increments. For each current value ι, the motor was run for 2 min to let the oscillator achieve its stable energy E. A 30 min chronometry test was then performed, as described in Section 4.2.1, to obtain a best fit period T^*. The best fit period T_0^* corresponding to ι_0 is considered the nominal rate. As described in Section 4.3.1, a rate ρ was then computed for each ι and compared to relative current variation which estimates the relative energy variation, see Fig. 30.

Finally, a linear regression was performed on the values of ρ as compared to the relative current variation $\iota_{\%}$, as shown in Fig. 30. The slope of this regression line was computed to be -2.2s/d/%.

5. Discussion

We discuss whether the goals given in Section 1.4 have been achieved.

- *Study the analytic theory of spherical 2-DOF oscillators and theoretical mechanisms realizing their kinematics.*

Section 2 gives an overview of the theory of 2-DOF spherical oscillators. The kinematic restriction to 2-DOF, Listing's Law, is well-known in the field of eye movements, but the dynamics described in Section 2.2 appear to be new.

The theoretical mechanisms described in Section 2.4 appear to be new, in particular, the observation that a constant velocity joint can be used to mechanize Listing's Law.

- *Use the ideal theoretical mechanisms as an inspiration for a simple mechanical design.*

The mechanical design described in Section 3 is very simple, only four beams are used for the suspension and the implementation of Listing's Law.

- *Provide an analytical model of the design.*

The analytical model of the design described in Section 3.3 uses a classical approach known to apply to the small amplitudes we examine.

- *Derive numerical data from the analytical model of the design.*

The numerical data given in Section 3.2 was validated by finite element analysis. This data shows that our three equatorial beams approach a scissors law. However, adding the polar beam produces a large deviation from the scissors law. We address this by stating that the theory was used as inspiration for our design and we did not necessarily intend this design to faithfully reproduce the theoretical model.

- *Construct a physical realization of the design.*

The physical realization of Section 4.1 was simple to construct as was its interface with the measurement apparatus also described in that section.

- *Evaluate the chronometric performance of the physical realization.*

The chronometric performance of the physical realization described in Sections 4.2 and 4.3 are promising since they are consistent with the performance of comparable horological time bases.

References

[1] Allan DW, Ashby N, Hodge CC. The science of timekeeping. HP Application Note 1289. Hewlett-Packard; 1997.
[2] Arnold RN, Maunder L. Gyrodynamics and its engineering applications. Academic Press; 1961.
[3] Awtar S, Slocum H, Sevincer E. Characteristics of beam-based flexure modules. J Mech Des 2007;129:625–39.
[4] Bonev I. Geometric analysis of parallel mechanisms (Ph.D. thesis). Université de Laval; 2002.
[5] Carpenter RHS. Movements of the eyes. 2nd ed. London: Pion; 1988.
[6] Constant-velocity joint, Wikipedia. en.wikipedia.org/wiki/Constant-velocity_joint [retrieved 08.06.16].
[7] Defossez L. Théorie Générale de l'Horlogerie, Tome I–II. La Chambre suisse d'horlogerie, La Chaux-de-Fonds 1950–1952; 1950–1952.
[8] Donders FC. Beitrag zur Lehre von den Bewegungen des menschlichen Auges. Holl. Beitr. Anat. Physiol. Wiss. 1848;1:104–45.
[9] Neuchâtel Clock for the 21st Century, Federation Horlogere. www.fhs.swiss/eng/2017_01_26_01_EPFL_Instant-Lab.html [retrieved 30.07.17].
[10] Goldstein H, Poole C, Safko J. Classical mechanics. 3rd ed. Addison-Wesley; 2000.
[11] Haslwanter T. Mathematics of three-dimensional eye rotations. Vis Res 1995;35:1727–39.
[12] von Helmholtz H. Helmholtz's Treatise on Physiological Optics. Southall JPC, editor. The Perceptions of Vision, Vol. III. Optical Society of America; 1925.
[13] Henein S. Conception des guidages flexibles. Presses Polytechniques et Universitaires Romandes; 2001.
[14] Henein S, Vardi I, Rubbert L, Bitterli R, Ferrier N, Fifanski S, Lengacher D. IsoSpring: vers la montre sans échappement, actes de la Journée d'Etude de la SSC. 2014. p. 49–58.
[15] Henein S, Vardi I, Rubbert L, XY isotropic harmonic oscillator and associated time base without escapement or with simplified escapement. European patent EP2894521; July 16, 2015.
[16] Henein S, Vardi I. The geometry of eye movement dynamics. J Eye Mov Res 2015;8(4):65.
[17] Howell LL. Compliant mechanisms. Wiley; 2001.
[18] Huygens C. Horologium oscillatorium [Latin with English translation by Ian Bruce]. www.17centurymaths.com/contents/huygenscontents.html [retrieved 09.06.14].
[19] Lagrange's trigonometric identities, Wikipedia entry. en.wikipedia.org/wiki/List_of_trigonometric_identities#Lagrange.27s_trigonometric_identities [retrieved 08.06.16].
[20] Lawden DF. Elliptic functions and applications. New York: Springer-Verlag; 2010.
[21] Martinez-Trujillo JC. Noncommutativity of eye rotations and the half-angle rule. Neuron 2005;47:171–3.
[22] Exposition temporaire – La neuchâteloise, exhibit May 6, 2017–October 8. Switzerland: International Museum of Horology, La Chaux-de-Fonds; 2017.
[23] Morin D. Introduction to classical mechanics. Cambridge University Press; 2007.
[24] Nakayama K. A new method of determining the primary position using Listing's law. Am J Optom Physiol Opt 1978;55:331–6.
[25] Newton I. The mathematical principles of natural philosophy [Translated by Andrew Motte 1729] vol. 1. Google eBook; 2014. [retrieved 09.06.14].
[26] Niaudet-Breguet. Application du diapason à l'horlogerie, Séance de lundi 10 décembre 1866. C. R. Acad. Sci. 1866;63:991–2.
[27] Perotto J-F. Les bases de temps horlogères. Bull Sociét Suisse Chronom 2009;61:21–6.
[28] Quaia C, Optican LM. Commutative saccadic generator is sufficient to control a 3-D ocular plant with pulleys. J Neurophysiol 1998;79:3197–215.
[29] Quaia C, Optican LM. Three-dimensional rotations of the eye. In: Levin LA, Nilsson SFE, Hoeve JV, Wu S, Kaufman PL, Alm A, editors. Chapter 8 of "Adler's physiology of the eye. 11th ed.Elsevier; 2011.
[30] Rubbert L, Bitterli RA, Ferrier N, Fifanski SK, Vardi I, Henein S. Isotropic springs based on parallel flexure stages. Precis Eng 2016;43:132–45.
[31] Rzeppa AH. Universal Joint. U.S. Patent 1,916,442; July 4, 1933.
[32] Taylor J. Classical mechanics. University Science Books; 2005.
[33] Tweed D. Visual-motor optimization in binocular control. Vis Res 1997;37:1939–51.
[34] Tweed DB, Haslwanter TP, Happe V, Fetter M. Non-commutativity in the brain. Nature 1999;399(20):261–3.
[35] Tweed D, Vilis T. Implications of rotational kinematics for the oculomotor system in three dimensions. J Neurophysiol 1987;58:832–49.
[36] Tweed D, Vilis T. Geometric relations of eye position and velocity vectors during saccades. Vis Res 1990;30:111–27.
[37] Vardi I. Le facteur de qualité en horlogerie mécanique. Bull Bull Sociét Suisse Chronom 2014;75:57–65.
[38] Whittaker ET. A treatise on the analytical dynamics of particles and rigid bodies. 4th ed. Cambridge University Press; 1988.
[39] Wittrick WH. The properties of crossed flexure pivots, and the influence of the point at which the strips cross. Aeronaut Q 1950;2(51):272–92.